



Highly efficient catalytic hydrogenation of nitrophenols by sewage sludge derived biochar

Xiaoya Ren^{a,b,1}, Lin Tang^{a,b,1}, Jiajia Wang^{a,b,1}, Eydhah Almatrafi^c, Haopeng Feng^b, Xiang Tang^b, Jiangfang Yu^b, Yang Yang^b, Xiaopei Li^b, Chenyun Zhou^{a,b}, Zhuotong Zeng^{a,b}, Guangming Zeng^{a,b,*}

^a Department of Dermatology, Second Xiangya Hospital, Central South University, Changsha 410011, PRChina

^b College of Environmental Science and Engineering, Hunan University and Key Laboratory of Environmental Biology and Pollution Control (Hunan University), Ministry of Education, Changsha 410082, PR China

^c Center of Research Excellence in Renewable Energy and Power Systems, Center of Excellence in Desalination Technology, Department of Mechanical Engineering, Faculty of Engineering-Rabigh, King Abdulaziz University, Jeddah 21589, Saudi Arabia

ARTICLE INFO

Keywords:

Sewage sludge
Biochar
Nitrophenol reduction
Graphitic N
Electron transfer

ABSTRACT

Finding a low cost and effective alternative to noble metal based catalyst has long been concerned in wastewater treatment and organic transformation. This work developed a highly efficient sewage sludge-based catalyst via a simple one-step pyrolysis method, and for the first time, applied it in the catalytic reduction of nitrophenols. Due to the higher content of graphitic nitrogen, abundant defect sites and low electron transfer resistance, sewage sludge derived biochar obtained at 800 °C (SSBC-800) exhibits the best catalytic performance, with the reaction rate of 0.48 min⁻¹ and turnover frequency for 4-nitrophenol calculated to be 1.25 × 10⁻⁴ mmol•mg⁻¹ min⁻¹, which is comparable to or even superior than some reported noble metal-based catalyst. Moreover, SSBC-800 showed good recyclability of 90% 4-nitrophenol removal within 8 min after 4 runs, and maintained high catalytic activity in reduction of other substituent nitrophenols, such as 2-nitrophenol (0.54 min⁻¹), 3-nitrophenol (0.61 min⁻¹) and 2,4-dinitrophenol (0.18 min⁻¹), and in real water samples, indicating its practical applicability. The electron paramagnetic resonance spectra and electrochemical characterization demonstrate that SSBC-800 accelerates the dissociation of BH₄⁻ to form active hydrogen, which is the main species responsible for 4-nitrophenol reduction, while electron transfer reaction involving the surface bound hydride derived from the intimate contact between BH₄⁻ and SSBC-800 plays an important role in this process. This research not only provides a novel valorization pathway for sewage sludge, but also sheds new light on further designing of carbon-based catalyst for nitrophenol reduction.

1. Introduction

Nitrophenols are a class of highly toxic and non-biodegradable organic pollutant commonly found in the waste effluents of dyeing, pesticide and pharmaceutical industries (Gupta et al., 2014; Oturan et al., 2000). It is highly desired to find a convenient and effective method for the removal of nitrophenols from aquatic environment, and catalytic hydrogenation is the most attractive one. The hydrogenation product aminophenols are less toxic, easier to be mineralized than nitrophenols. More importantly, aminophenols can be used as chemical intermediates for the synthesis of pharmaceuticals, dyes, corrosion

inhibitor, agrochemicals and imaging agents, which bring economic benefits (Vaidya et al., 2003; Xia et al., 2016). Therefore, conversion of nitrophenols into value added aminophenols is of great importance both in environmental remediation and industrial synthesis (Cao et al., 2020; Das et al., 2019).

In the hydrogenation reduction of nitrophenols, noble metal based catalysts (e.g., Ag, Au, Pd and Pt) firstly attract widespread attention due to their high catalytic efficiency (Fu et al., 2018, 2019; Gao et al., 2018; Xi et al., 2016). However, the excessive cost and limited supplies of noble metals restricted their large scale application. Besides, metal-based catalysts tend to suffer from problems of poor durability,

* Corresponding author.

E-mail addresses: zengzhuotong@csu.edu.cn (Z. Zeng), zgming@hnu.edu.cn (G. Zeng).

¹ These authors contribute equally to this article.

easy agglomeration and metal leaching, which could cause deactivation of the catalyst and secondary pollution (Wang et al., 2018). In comparison, carbocatalyst is an ideal candidate owing to the high stability, readily availability, environmental friendliness and biocompatible (Ren et al., 2021; Yang et al., 2020). Several carbon-based catalysts such as reduced graphene oxide (Hu et al., 2015), boron and nitrogen-doped porous carbons (Van Nguyen et al., 2019) and nitrogen-doped graphene (Kong et al., 2013) have been proved to show certain catalytic ability in the hydrogenation reaction. However, the preparation processes of those carbon-based catalysts are complicated and their catalytic efficiency is inferior to metal-based catalyst. It is essential to find an economic and highly efficient carbon-based catalyst for this application.

Sewage sludge is a mass produced byproduct of wastewater treatment, with an estimation of 40 million tons every year (Yang et al., 2015a). Conversion of sewage sludge into functional catalyst such as biochar is a promising method, not only for sludge disposal, but also for low cost catalyst preparation (Cieslik et al., 2015). Until now, sewage sludge-based carbon materials has been explored for some applications, such as adsorbent (Smith et al., 2009), capacitance materials (Xu et al., 2020) and persulfate activation (Yu et al., 2019). However, less attention has been given on the field of catalytic hydrogenation. It is well documented that pristine carbon material is almost inert for the hydrogenation reaction due to the deficient of active site but introduction of heteroatom, especially nitrogen atoms, can modulate the charge distribution of the carbon structure and create new charged site (Yang et al., 2015b). For example, Kong et al. (2013) found that the pure graphene was inactive in the 4-nitrophenol (4-NP) reduction while N-doped graphene displayed high catalytic efficiency in this reaction, with the carbon atom adjacent to the doped nitrogen atom serving as the reactive site. In addition, as the catalytic hydrogenation of nitrophenols is a reduction process, the catalyst with high electron transfer ability must be beneficial for the reaction. Sewage sludge is a complex matrix with abundant organic matter and inorganic minerals. Specially, the microorganisms and extracellular polymeric substances in sewage sludge provide the possibility of nitrogen doping (Parnaudeau and Dignac, 2007; Syed-Hassan et al., 2017). The nitrogen species in the sewage sludge could form active C–N bond after high temperature carbonization, thus providing the possible site for the hydrogenation reaction. Meanwhile, during pyrolysis, the conductive graphitic carbon lattice was gradually formed within the biochar, which is favorable for fast electron transfer (Zhang et al., 2018). It is therefore supposed that the sewage sludge-derived biochar (SSBC) also exhibit high catalytic activity for this organic reaction.

This study aims to demonstrate the feasibility of SSBC as a catalyst in the hydrogenation reduction of 4-NP. Considering the unique structure properties (e.g. N doping and graphitic structure) and the advantage of waste recycling, the SSBC is expected to be a promising low cost and powerful alternative to noble metal-based catalyst for nitrophenols reduction. The impact of pyrolysis temperature on the specific surface area, pore size, surface chemistry and correlative catalytic performance is investigated. The catalytic active site inside the biochar and possible reaction mechanism of 4-NP reduction are explored. Moreover, the effectiveness in real water samples and the reduction of other nitrophenols (e.g. 2-NP, 3-NP and 2,4-DNP) are also studied to verify the practical applicability.

2. Materials and methods

2.1. Chemicals and materials

Sodium borohydride (NaBH_4), 4-nitrophenol (4-NP), 2-nitrophenol (2-NP), 3-nitrophenol (3-NP), 2,4-dinitrophenol (2,4-DNP) were purchased from Sinopharm Chemical Reagent Co. Ltd (Shanghai, China). All the chemical reagents were of analytical grade and used as received without further purification.

2.2. Preparation of sewage sludge-derived biochar

The municipal sewage sludge used in this study was collected from Kingsha wastewater treatment plant in Changsha, China. The obtained solid was firstly dried in the oven at $105\text{ }^\circ\text{C}$ for 72 h, then grounded and sifted through 100 mesh sieves for further use. Subsequently, the sample was carbonated in a tubular furnace at the designed temperature for 120 min under constant nitrogen flow (heating rate: $5\text{ }^\circ\text{C}/\text{min}$, nitrogen flow rate: 100 mL/min). The final products pyrolyzed at the temperature of 400, 600, 800 and $1000\text{ }^\circ\text{C}$ were denoted as SSBC-400, SSBC-600, SSBC-800 and SSBC-1000, respectively.

2.3. Catalytic reduction of nitrophenols

The catalytic performance of as-prepared sewage sludge-derived biochar was evaluated by reduction of nitrophenols in the presence of NaBH_4 . Typically, 10 mg of SSBC was added to 50 mL of freshly prepared 4-NP aqueous (0.2 mM) solution followed by adding 0.076 g of NaBH_4 under continuous stirring at room temperature. At a certain time interval, 2.5 mL of the reaction solution was withdrawn, filtrated with $0.45\text{ }\mu\text{m}$ filter membrane, and measured using UV–Vis spectrophotometer at the absorbance wavelength of 400 nm. For the recycling test, after each reaction, the catalyst was separated by centrifuge (8000 rpm, 30 min), rinsed several times with ultrapure water and then dried in an oven for 24 h before the next reaction. The reduction of other nitrophenols was conducted following the same procedure of 4-NP. Adsorption evaluation of 4-NP was carried out as the same conditions of catalytic test without the addition of NaBH_4 . An additional sorption isotherms experiment with SSBC-800 was also performed to investigate the adsorption behavior of 4-NP (Details can be seen in Text S1). In addition, the catalytic activity of SSBC in real water sample, including tap water, lake water and river water (respectively collected from laboratory, Lake of Peach, and Hsiang River in Changsha, China) was also conducted. All those water samples were filtered with $0.45\text{ }\mu\text{m}$ membrane to remove the impurities. Detailed information about those water samples were provided in Table S1.

2.4. Characterization

The morphology of the catalyst was characterized by scanning electron microscope (SEM, Zeiss Merlin). Fourier transform-infrared spectroscopy spectra (FTIR, spectrum GX USA) within the wavenumbers ranging from $400\text{ to }4000\text{ cm}^{-1}$ was used to investigate the surface functional group. The specific surface area (SSA) and pore size distribution were acquired from the nitrogen adsorption-desorption isotherm curve conducted on the Quantachrome NovaWin (NOVA 2000e). X-ray diffraction (XRD) were examined on Bruker D8 Advance using Ni-filtered $\text{Cu K}\alpha$ radiation ($\lambda = 1.54\text{ \AA}$). X-ray photoelectron spectra (XPS) was carried out by a Thermo Escalab 250 instrument under an Al-K α X-ray radiation to study the element composition. The element content was determined using an elemental analyzer (Vario Micro Cube). Zeta potential was determined with the Zeta-sizer Nano-ZS (Malvern). Electron paramagnetic resonance (EPR) spectra were conducted on the Bruker EMX-A300. Raman spectra were obtained using the LabRAM HR800 at the excitation wavelength of 532 nm. Electrochemical measurements including the electrochemical impedance spectroscopy and chronoamperometry were performed on a CHI 760E electrochemical workstation and details were shown in Text S2. The UV–vis spectrum was recorded with a UV-2700 spectrophotometer (Shimadzu, UV-3600).

3. Result and discussion

3.1. Characterization of sewage sludge-derived biochar

The N_2 adsorption/desorption curves were conducted to determine

the SSA of SSBC, and related dates were presented in Table S2. The SSA of SSBC400 was 44.15 m²/g, and the value increased to 49.33 m²/g, 62.29 m²/g, 98.47 m²/g for SSBC-600, SSBC-800 and SSBC-1000, respectively (Table S2). During the pyrolysis of biomass, three products were generated: solid carbon matrix (i.e., biochar), volatile organic matters (e.g., bio-oil) and “non-condensable” gases (e.g., CO, CO₂, CH₄, H₂, H₂S) (Kambo and Dutta, 2015). With the increase of pyrolysis temperature, the biomass molecular evolves towards a condensed structure, along with the release of more organic matters and gasses from carbon matrix, which may be the main reason for the larger SSA of SSBC-1000 (Collard and Blin, 2014). Generally, higher total pore volume and SSA could provide more active sites for the reaction and absorb more reactants, thus resulting in a higher reactive activity. As shown in Fig. 1a, the nitrogen adsorption/desorption isotherms were in type IV model along with a distinct H2 hysteresis loop, implying the existence of mesoporous network. This was consistent with the pore-size distribution plot, with the average pore diameter of SSBC in the range of 5.6–7.5 nm (Fig. S1). The mesoporous structure is beneficial to the diffusion of reactants and provides more access to inner reactive site during the catalysis process (Yang et al., 2015b).

The surface functional group of SSBC was revealed by FTIR spectra in Fig. 1b. With the increase of pyrolysis temperature, the intensity of peak corresponding to O–H stretching (3624 cm⁻¹), N–H asymmetric stretching (3417 cm⁻¹), –CONH– (1433 cm⁻¹) and C–O/C–N (1023 cm⁻¹) gradually decreased or even disappeared, indicating the decomposition /fracture of carbohydrates and amino acid in sewage sludge during the calcination process. The same decreasing trend was also observed for the bond of aliphatic C–H stretching at 2853–2964 cm⁻¹ due to the demethylation and dehydration reaction (Zhang et al., 2015). Meanwhile, the development of C=C stretching vibration (1584 cm⁻¹) together with the reduction of C=O stretching vibration (1614 cm⁻¹) was observed at temperature above 600 °C, which suggested the increased graphitization at higher pyrolysis temperature (Yu et al., 2019). The weaker intensity of SSBC-1000 at 688 cm⁻¹ and 785 cm⁻¹ for aromatic C–H wagging vibrations than that of SSBC-400 also indicated the intensified polymerization at SSBC-1000 (Zhang et al., 2018). Besides, the peak belonging to Si-O vibration at 1089 cm⁻¹ was detected,

implying the existence of inorganic minerals in SSBC (Zhang et al., 2015). Similarly, the XRD pattern also showed that except for carbon, SiO₂ with the characteristic value of around 26.6°, was observed for all the SSBC samples (Fig. 1c). The origin of SiO₂ in SSBC was probably from the inorganic minerals such as glass and sand inherent in sewage sludge.

Raman spectroscopy was carried out to identify the structure change of SSBC (Fig. 1d). All the samples exhibit three typical peaks, namely a D band at about 1379 cm⁻¹, a G band at about 1597 cm⁻¹, and a 2D band at about 2800 cm⁻¹. Generally, the D peak (breathing vibration mode, A_{1g} symmetry) is associated with defect edges of the graphitic carbon, and the G peak (Tangential Mode, E_{2g} symmetry) is typically assigned to the graphite structure (Keown et al., 2007). The ratio of I_D/I_G is expected to decrease with pyrolysis temperature due to the increased extent of graphitization. But it is not the same for biomass derived carbon. From the graphite (g-C) to tetrahedral amorphous carbon (ta-C), the amorphization trajectory divided it into three-stage: g-C to nanocrystalline graphite (ng-C); ng-C to amorphous one (a-C); and a-C to ta-C (Robertson and Ferrari, 2000). The transition process of SSBC could be in the reverse direction of stage 2 due to the presence of 2D band and the blue shift of G band from 1581 cm⁻¹ (characteristic position of graphite) to 1597 cm⁻¹ (Fig. 1d). Therefore, the D and G band in this study showed different features from graphite. The D band and G band of SSBC were broad and overlapped especially in low pyrolysis temperature, implying the multiphase of SSBC (McDonald-Wharry et al., 2013). During the process of carbonization, the biomass went through dehydrogenation, polymerisation and condensation and become increasingly aromatic. The aromatic clusters generated by the stacks of aromatic molecules were graphitic-like, and is generally termed as nanocrystalline. Therefore, the microstructure of SSBC can be regarded as nanocrystallites (sp² carbon) embedded in the amorphous matrix (Tsaneva et al., 2014). In this case, the D band in SSBC could be ascribed to the vibration of sp²-bonded carbon atoms in hexagonal aromatic rings, and the development of D band represents greater structure ordering, while the G band is likely to be aromatic ring breathing rather than E_{2g} vibrations of crystalline graphite (Keown et al., 2007). Due to the incomplete carbonization, large numbers of small aromatic ring still

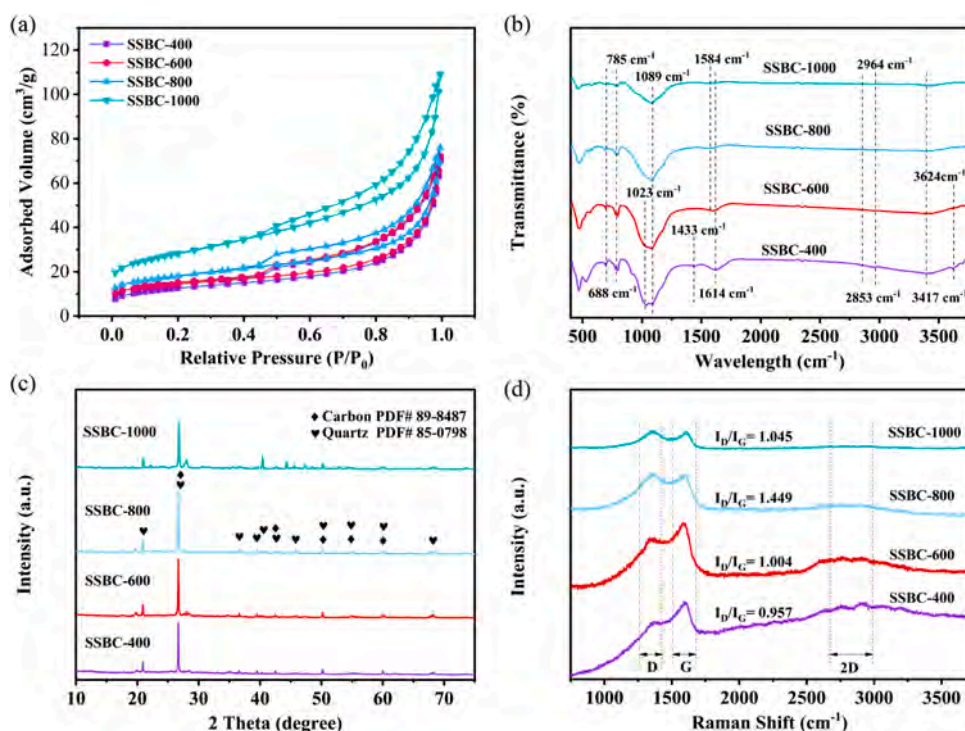


Fig. 1. (a) N₂ adsorption-desorption isotherms of SSBC; (b) FTIR spectra of SSBC; (c) XRD pattern of SSBC; (d) Raman spectra of SSBC.

exist in SSBC-400. Accordingly, the increment of I_D/I_G from 400 to 800 °C was attributed to the increasing proportion of larger aromatic rings (with at least six rings) in SSBC. However, at higher pyrolysis temperature of 1000 °C, the I_D/I_G of the sample decreased, which could be the competition between ring growth and decrease in structure defects, manifesting further approach of biochar structure to graphite.

The element composition of SSBC was shown in Table S2. It can be seen that with the increase of pyrolysis temperature, the content of C, H, O and N has gradually decreased, which is ascribed to the decomposition of organic molecules within the sewage sludge. Meanwhile, the H/C, N/C and O/C ratio dropped steadily with pyrolysis temperature, indicating the gradual carbonization and aromatization of SSBC (Zhang et al., 2015). The XPS survey proved the existence of carbon, nitrogen, oxygen element (Fig. S2), which was consistent with the result of EDS-mapping (Fig. S3). The deconvolution of C1s spectrum exhibited four peaks at about 284.74 eV, 285.78 eV, 287.30 eV, and 288.96 eV, which corresponding to C—C/C=C, C—OH/C—N, C=O/C=N and π - π^* shake up, respectively (Fig. S4). Noteworthy, the π - π^* shake up only appeared at the temperature above 600 °C, and the content increased from 2.48% (SSBC-600) to 3.57% (SSBC-1000), which indicated the improved graphitization at higher pyrolysis temperature. This is consistent with the decreasing ratio of O/C from 0.71 to 0.29 (Table S1). Heteroatom nitrogen has been reported as active site for hydrogenation reaction. The high-resolution N1s spectrum can be divided into four peaks, i.e., pyridinic N (around 398.67 eV), pyrrolic N (around 400.44 eV), graphitic N (around 401.21 eV) and oxidized-N (around 403.55 eV) (Fig. 2). In SSBC-400, the nitrogen species display as pyridinic N (21.87%) and the pyrrolic N (78.13%). With an enhanced pyrolysis temperature to 600 °C, a new peak assigning to graphitic N emerged and the relative content increased from 9.05% (SSBC-600) to 71.94% (SSBC-800) and further to 90.09% (SSBC-1000). Meanwhile, the fraction of pyrrolic N gradually decreased and eventually disappeared at the temperature above 800 °C, which indicates the transformation order of N species from pyrrolic N to pyridinic N and finally to graphitic N. It is well known that graphitic N has higher thermal stability than the other

two nitrogen species.

3.2. Catalytic performance of SSBC for nitrophenols reduction

The catalytic activity of SSBC was evaluated by hydrogenation reduction of 4-NP with NaBH_4 and the reaction was investigated by UV-vis spectroscopy. Upon the addition of NaBH_4 , the maximum absorption peak of 4-NP shifted from 317 nm to 400 nm, along with the color change from light yellow to dark yellow, which is ascribed to the transformation of 4-nitrophenol to 4-nitrophenolate ion under alkaline conditions (Fig. S5a) (Qiu et al., 2014). Obviously, NaBH_4 alone was incapable of reducing 4-NP due to the kinetic barrier (Fig. S5b). After addition of SSBC-800, the absorption peak at 400 nm diminished and vanished finally, while a new absorption peak at 300 nm that derived from 4-aminophenol (4-AP) emerged and became gradually intensified (Cao et al., 2020). Simultaneously, as the reaction proceeded, the color of the system turned from yellow into colorless (Fig. 3a). These results demonstrated the successful reduction of 4-NP to 4-AP by SSBC-800.

As pyrolysis temperature largely affect the property of biochar, the catalytic hydrogenation of 4-NP by different SSBC was studied (Fig. S5c). SSBC-400 was nearly inert for the reaction, while SSBC-600 showed 58% conversion of 4-NP within 20 min. Significantly, SSBC-800 presented a promising catalytic activity of 100% 4-NP conversion at 8 min (Fig. 3a and Fig. S5c). However, compared to SSBC-800, further increasing the pyrolysis temperature to 1000 °C resulted in a slight decrease in 4-NP conversion. Fig. 3b showed the kinetic plots of the reduction reactions. The approximately linear relationship between $\ln(C_t/C_0)$ versus time demonstrated well fit of the reaction by pseudo-first-order kinetics. The calculated reaction rate constant K_{app} for SSBC-600, SSBC-800 and SSBC-1000 was 0.046, 0.48 and 0.26 min^{-1} , respectively. Turn over frequency (TOF), which was defined as the amount of reactant molecules converted to products by per unit mass of catalyst per minute, was used to assess the catalytic efficiency. The TOF of SSBC was calculated to be $1.25 \times 10^{-4} \text{ mmol} \cdot \text{mg}^{-1} \cdot \text{min}^{-1}$, which was comparable to and even superior to some reported noble metal-based catalyst, such as

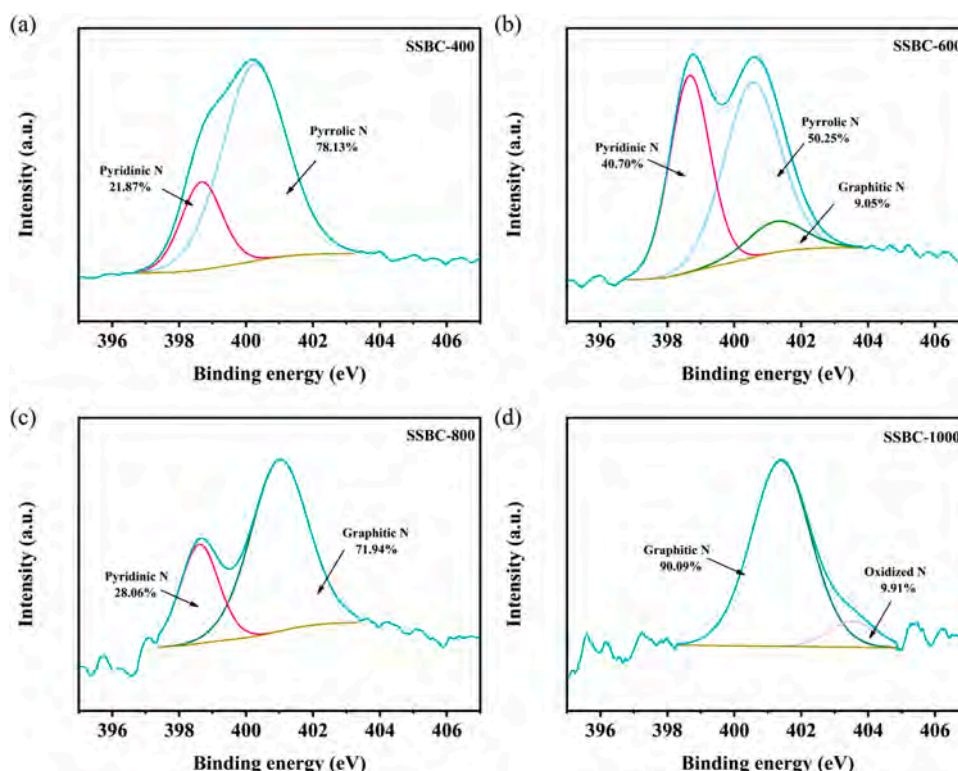


Fig. 2. High-resolution XPS spectrum in N1s region for (a) SSBC-400, (b) SSBC-600, (c) SSBC-800, and (d) SSBC-1000.

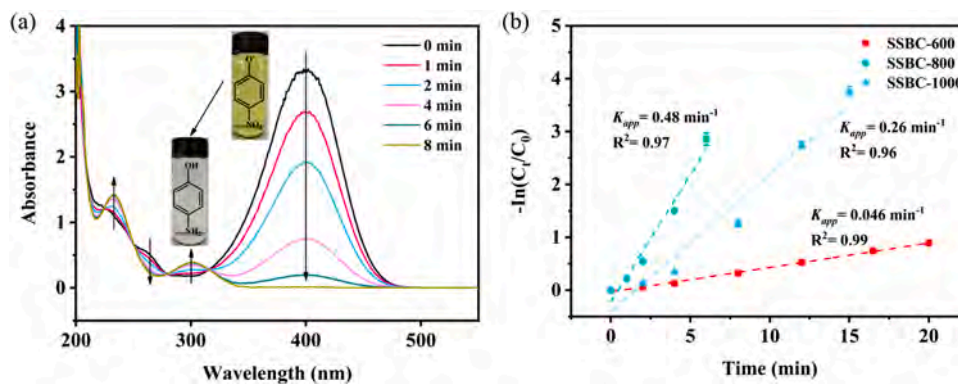


Fig. 3. (a) Time-dependent UV-vis absorption spectra of 4-NP catalytic reduction by SSBC-800; (b) Plots of $-\ln(C_t/C_0)$ versus time for 4-NP reduction by different SSBC.

Au@C (1.2×10^{-5}) (Liu et al., 2011), Ag@PEI@AHB (4.4×10^{-5}) (Gao et al., 2018) and Pd-CNT-rGO (1.2×10^{-4}) (Zhang et al., 2014) (Table S3). Noteworthy, compared with those noble metal-based materials with high cost and complicated production process, the raw material used in this study was derived from the industrial waste sewage sludge and the preparation process was much simple and cost-effective (Text S2).

3.3. Possible mechanism

To determine whether the reaction process follows the Eley-Rideal mechanism or the Langmuir-Hinshelwood mechanism, the dependence of K_{app} on the concentration of 4-NP and NaBH_4 is investigated. Fig. S6 showed a nonlinear relationship between them, and the K_{app} increased with the increasing concentration of NaBH_4 while gradually decreased with 4-NP. In the Eley-Rideal model where only one of the reactants adsorbed on the catalyst surface, the K_{app} was supposed to increase as the rising of 4-NP concentration. This is contradictory with the experiment results. The entire process was more suited to the Langmuir-Hinshelwood model, which illustrated that both the 4-NP and BH_4^- adsorbed on the catalyst before interfacial electron transfer (Narayanan and Devaki, 2015). In this case, 4-NP at higher concentration led to a larger coverage of the catalyst surface and left with little accessible surface for the BH_4^- , which consequently inhibit the reaction rate. This can be further confirmed by the fitting results of adsorption isotherms as shown in Fig. S7. Instead, a higher concentration of NaBH_4 makes more BH_4^- occupy on the catalyst surface and thus accelerates the reaction.

To further illustrate the possible reaction process in the SSBC/ NaBH_4 /4-NP system, EPR spectra with 5,5-Dimethylpyrroline N-oxide (DMPO) as the spin trapper was conducted to demonstrate the existence of H radical species. As shown in Fig. 4a, no signal appeared in the

mixture solution of 4-NP and SSBC-800. After addition of NaBH_4 , an obvious signal that consisted of a 1:1:1 triplet of 1:2:1 triplet ($a_H=22.57$ G and $a_N=16.62$ G) were detected, which was assigned to the DMPO-H adduct (Nguyen et al., 2019). It is proposed that the active H species is derived from the dissociation of B-H bond and SSBC accelerate the abstraction of hydrogen. This is consistent with the results of chronoamperometric test (Fig. 4b). Addition of NaBH_4 or 4-NP had no obvious influence on the current output with bare electrode. Interestingly, a significant current response was observed after the injection of NaBH_4 with the SSBC-800 electrode, which was probably ascribed to the strong interaction between SSBC-800 and NaBH_4 . It was supposed that SSBC-800 stimulated the hydrogenation of NaBH_4 to form more hydride on the surface of SSBC-electrode. Besides, the current increase was also detected after 4-NP addition, due to the electron transfer from SSBC to 4-NP. Based on the above discussion, a reasonable catalytic mechanism is presented, which follows the Langmuir-Hinshelwood model (Scheme 1). BH_4^- reacts with the active site of SSBC to form the surface bound hydride. In the meantime, 4-NP is adsorbed onto the surface of SSBC-800 and captures the active hydrogen species and electrons from hydride complex. Finally, the generated 4-AP desorbs from the active sites. In this process, the catalyst function as the adsorption sites for reactant molecules, and electron transfer system between electron donor (BH_4^-) and electron acceptor (4-NP).

As the K_{app} of SSBC follows the order of SSBC-800 > SSBC-1000 > SSBC-600 > SSBC-400, we now discuss some possible factors affecting the catalytic activity. Larger pore size is favorable for the mass transportation of reactant to the inner reaction site of catalyst. However, it can be observed from Fig. S1 that all the SSBC sample have similar pore size. Pore size can't be the reason for the catalytic difference of SSBC. With the increasing of pyrolysis temperature, the specific area of SSBC increased slightly from 44.15 to 98.47 m^2/g (Table S2). Higher surface

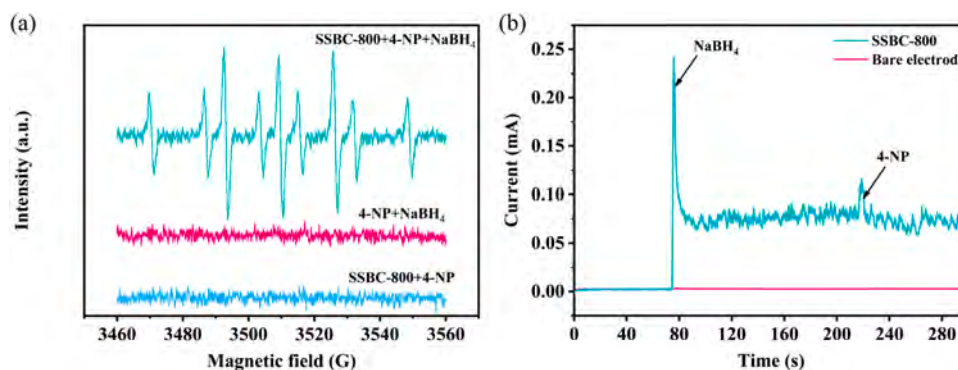


Fig. 4. (a) EPR spectra of DMPO-H adducts formed in the presence of SSBC-800+4-NP, 4-NP+ NaBH_4 and SSBC-800+4-NP+ NaBH_4 ; (b) I-t curves of SSBC-800 loaded electrode and bare electrode.

area would increase the adsorption of 4-NP and thus facilitate the reaction rates. The adsorption capacity of SSBC follows the order of SSBC-1000 > SSBC-800 > SSBC-600 > SSBC-400 (Fig. S8). The enhanced surface area may partly explain the higher catalytic activity of SSBC-800 and SSBC-1000 but can't explain the exceptional catalytic activity of SSBC-800 (Fig. S8a).

As mentioned above, electron transfer is an essential process for the reduction conversion of 4-NP. The charge-transfer capacity of SSBC is assessed by the electrochemical impedance spectroscopy (EIS), among which the semicircle diameter represents the interfacial charge-transfer resistance (Fig. S9b). As expected, the conductivity of SSBC increases with the pyrolysis temperature. A significant decrease of semicircle size can be found when pyrolysis temperature of SSBC rising from 600 °C to 800 °C. In this stage, the aromatic rings are largely formed and thus SSBC-800 exhibits a much higher degree of graphitization than SSBC-600. Compared with amorphous carbon, graphitic carbon is more favorable for electron transfer. However, SSBC-1000 with higher conductivity showed lower K_{app} than SSBC-800, indicating that conductivity was not a determining factor for the catalytic hydrogenation of 4-NP. It is proposed that the high reactivity is derived from the active site in SSBC.

To exclude the effect of trace leaching metals on the catalytic hydrogenation of 4-NP, the dissolved fraction of SSBC-800 was extracted for this reaction. No decrease of 4-NP absorption peak was observed in Fig. S10a, demonstrating the negligible contribution of leaching metals to the 4-NP removal. Besides, it was found that SSBC-800 after acid treatment (rinsed with 2 M HCl for 48 h to remove the metal impurities) exhibited comparable catalytic activity with the original one (Fig. S10b). Thus, we suppose that the as prepared carbon materials provide the catalytic site for this reaction. Previous studies reported that the carbon atom next to doped nitrogen could act as the catalytic site in the reduction reaction of 4-NP (Kong et al., 2013; Wang et al., 2017). Introduction of heteroatoms nitrogen in the carbon frame induces the charge redistribution of the adjacent carbon atoms, and endows it with metallic electronic structure and desirable activity. In our study, the change of catalytic activity as the increasing of pyrolysis temperature was probably ascribed to the transformation of N doping forms in SSBC. Pyridinic N and pyrrolic N present a weak correlation with the value of K_{app} (Fig. S9c and d). However, a proximately positive liner relationship between the content of graphitic N and K_{app} was observed, implying the significance of graphitic N in this reaction (Fig. 5a). This is consistent with previous studies. (Yang et al., 2015b) and Shan et al. (2019) also found a high correlation between the catalytic activity of 4-NP reduction and the content of graphitic N. Yang et al. (2016) demonstrated that graphitic N exhibited the lowest adsorption energy with nitroarenes and the longest N–O bonds, which may be the reason for its higher catalytic activity than other type of nitrogen species in the N-doped graphene. In addition, the defect is an active adsorption site for hydrogen molecules (Hu et al., 2015, 2020). The higher ratio of I_D/I_G in SSBC-800 than

SSBC-1000 indicates lower level of regularity and a higher defect density in SSBC-800, which might also contribute to its higher catalytic activity (Fig. 5b). Moreover, since the catalytic hydrogenation of 4-NP proceeds when both the reactants diffuse and adsorb onto the surface of catalysts, adsorption of reactants on the surface of SSBC is a critical step for the catalytic reaction. As both the 4-nitrophenolate and BH_4^- are negative charged in the reaction solutions, the catalyst with higher zeta potential should have stronger attraction for the reactants. The zeta potential of SSBC follows the order of SSBC-800 > SSBC-600 > SSBC-1000, which could partly explain the higher catalytic activity of SSBC-800 (Table S4). Based on above discussions, the exceptional activity of SSBC-800 can be attributed to the high graphitic N content, abundant defects site and relative higher zeta potential.

3.4. Catalytic reduction of different nitrophenols

To explore the universality of SSBC-800 catalyst, the catalytic hydrogenation of other nitrophenols was also conducted. Fig. 6a-c showed that all the nitrophenols were converted efficiently. The strong absorption peaks of 2-NP (414 nm), 3-NP (393 nm), 2, 4-DNP (448 nm) decreased gradually as the reaction proceeded, and new peaks belonging to the reaction products appeared. The color of all reaction mixture changed to colorless finally, indicating the complete hydrogenation of them. As shown in Fig. 6d, the K_{app} of nitrophenols are in the order of 3-NP > 2-NP > 4-NP > 2, 4-DNP, which is attributed to the combined effect of conjugation, inductive and steric effect. It is generally believed that 2-NP and 4-NP have a relatively stable group due to the conjugation effect that makes the negative charge of the phenoxide ion delocalized onto the nitro group. In terms of the inductive effect, 2-NP with shorter distance between -OH and -NO₂ is supposed to have stronger inductive effect than 4-NP and such interactions result in more positively charged nitrogen atoms in 2-NP. In the hydrogenation reaction, nitrogen atom with positive charge is easier to be attacked by the negative charged active hydrogen and thus 2-NP have high reactivity than 4-NP. As to the 3-NP, no direct conjugation effect happens and the stabilization of nitro group only relies on the weak inductive effect (Guo et al., 2016). As a result, 3-NP has higher reactivity than 2-NP and 4-NP. In addition, compared with mononitrophenol, 2,4-DNP has larger steric resistance and is expected to exhibit the lowest reactivity (Sun et al., 2014).

3.5. Catalyst stability

The reusability of the catalysts is an important factor for the potential application. As displayed in Fig. 7a, after recycled for 4 times, SSBC-800 remains 90% removal of 4-NP within 8 min, indicating the good durability. The XRD pattern of used SSBC-800 presents no much difference from the fresh one (Fig. S11a). The I_D/I_G of spent SSBC-800 is 1.416, similar to SSBC-800 (Fig. S11b). The partial deactivation of SSBC-800 was probably caused by the adsorption of reaction products. After

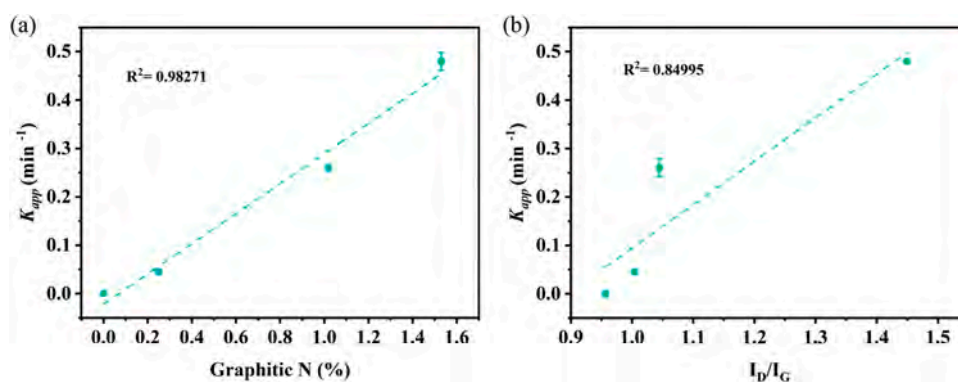


Fig. 5. (a) Relationship between reaction rate constant K_{app} and graphitic N content; (b) Relationship between reaction rate constant K_{app} and the value of I_D/I_G .

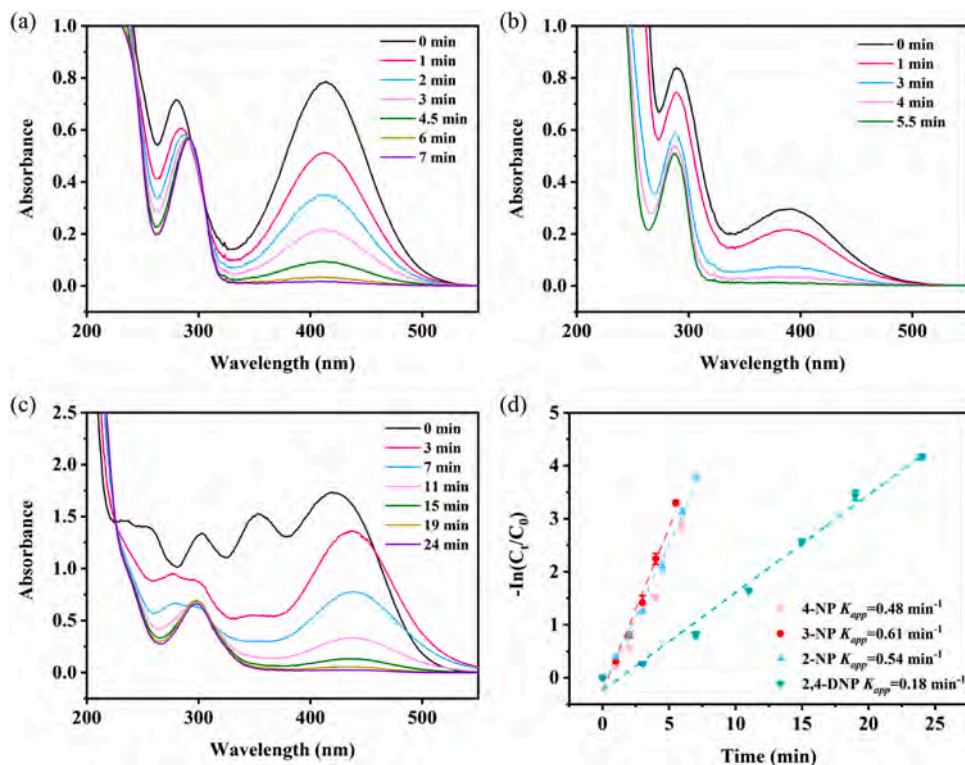


Fig. 6. Time-dependent UV-vis absorption spectra of (a) 2-NP, (b) 3-NP, (c) 2,4-DNP catalytic reduction by SSBC-800; (d) Plots of $-\ln(C_t/C_0)$ versus time for the reduction of nitrophenols by SSBC-800.

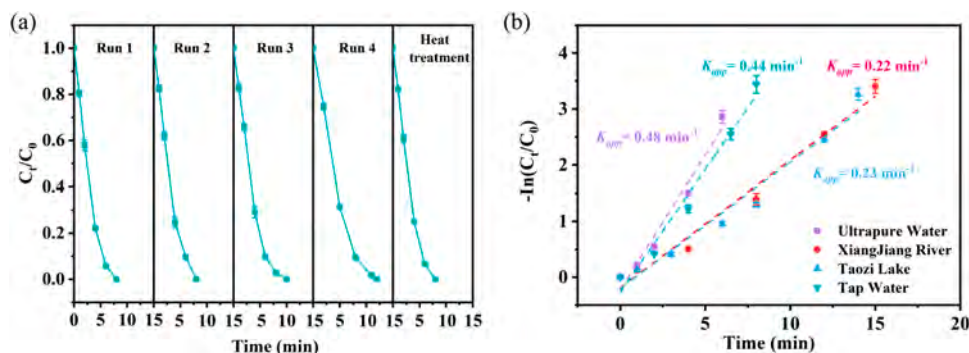


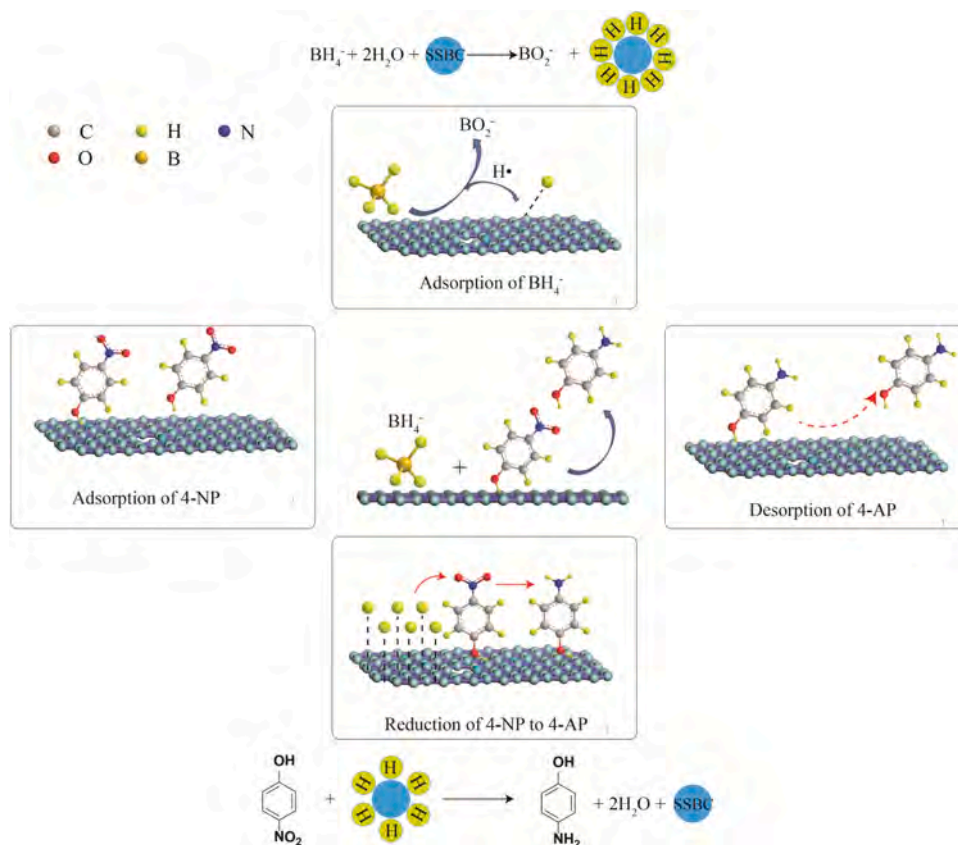
Fig. 7. (a) Reusability of SSBC-800; (b) Plots of $-\ln(C_t/C_0)$ versus time for the reduction of 4-NP by SSBC-800 in different water samples.

mild heat treatment at 350°C , the catalytic activity of SSBC-800 can be perfectly recovered.

3.6. Applicability in environmental water samples

To estimate the catalytic efficiency of SSBC-800 in real aquatic systems, reduction of 4-NP in different water samples including tap water, lake water and river water were also performed. The K_{app} in different water sample follows the order of ultrapure water > tap water (0.44 min^{-1}) > lake water (0.23 min^{-1}) > river water river water (0.22 min^{-1}). It has been reported that dissolved oxygen (DO), ions, solution pH and natural organic matter could affect the reaction process. To investigate the impact of DO, the catalytic reduction of 4-NP was conducted with N_2 protected. Fig. S12a showed no significant difference in 4-NP removal between the N_2 conditions and atmosphere conditions. Besides, it was found that inorganic ions (including Cl^- , SO_4^{2-} and NO_3^-), K^+ and Na^+ had negligible impact on the reduction of 4-NP (Fig. S12b). Interestingly, the presence of Ca^{2+} and Mg^{2+} slightly accelerated this

reaction. It was speculated that Ca^{2+} and Mg^{2+} could stimulate the hydrogen release from NaBH_4 , and thus provided more hydrogen resource for active H formation. Previous study also reported that alkaline earth metal halide could enhance the reactivity of NaBH_4 (Periasamy and Thirumalaikumar, 2000). Therefore, it was proposed that the lower K_{app} in real water samples was ascribed to the different solution pH (Table S1). To prove this hypothesis, the effect of pH on the reduction of 4-NP by SSBC-800 was investigated. As presented in Fig. S12c, with the increasing of solution pH from 3.71 to 9.12, the K_{app} decrease from 0.55 min^{-1} to 0.43 min^{-1} . Since the reduction of 4-NP follows the Langmuir-Hinshelwood model where adsorption of reactants is a critical step, the stronger adsorption attraction contributes to higher catalytic activity. The $\text{pH}_{\text{SSBC-800}}$ is at about 3.8, which means that the surface of SSBC-800 is negative charged at $\text{pH} > 3.8$ (Fig. S13). Meanwhile, 4-NP exists dominantly in the form of nitrophenolate anionic at $\text{pH} > 7$. Therefore, the alkaline environment of lake water ($\text{pH} 7.58$) and river water ($\text{pH} 7.65$) would weaken the adsorption force among SSBC-800, BH_4^- and 4-NP, consequently reducing the catalytic



Scheme 1. Proposed mechanism of 4-NP reduction in the presence of NaBH_4 by SSBC-800.

activity. Moreover, at higher solution pH, the surface of SSBC-800 was more negative charged, resulting in a larger electrostatic repulsion between BH_4^- and SSBC-800. In this case, the K_{app} in real water samples is lower than ultrapure water. However, it can be seen that the impact of pH on the catalytic reduction of 4-NP was not significant and cannot fully explain the much lower K_{app} in lake water and river water. Natural organic matter is a common interfering substance in water and humic acid (HA) is selected as the representative organic matter to evaluate its influence on 4-NP reduction. Introduction of HA had impeded the reduction of 4-NP, and the K_{app} decrease from 0.48 min^{-1} to 0.17 min^{-1} in the range of 0–40 mg/L HA (Fig. S12d). The inhibition effect was probably attributed to the competition between HA and reactants for available site on SSBC-800 (Wang et al., 2019). According to Table S1, the total organic carbon of lake water and river water is much higher than ultrapure water, which may be the main reason for its lower K_{app} . Noteworthy, although the K_{app} is suppressed in real water samples to some extent, as shown in Fig. S14, 4-NP can be still completely converted in a relatively short time, demonstrating the feasibility of SSBC-800 in practical application.

4. Conclusions

Based on the concept of “changing waste to wealth”, sewage sludge was used as the precursor to prepare a highly efficient carbocatalyst by direct thermal treatment for the catalytic hydrogenation of nitrophenols.

The impact of pyrolysis temperature on the structure and the subsequent catalytic efficiency of SSBC were investigated. SSBC-800 possesses high content of graphitic nitrogen, abundant defects site and good electron transfer capacity, which is favorable for the hydrogenation reaction.

The TOF of SSBC-800 for 4-NP reduction ($1.25 \times 10^{-4} \text{ mmol} \cdot \text{mg}^{-1}$

min^{-1}) is comparable with some reported noble metal based catalyst, but possessing the advantage of lower cost and simpler synthesis route.

Moreover, SSBC-800 shows good recyclability (90% 4-NP conversion within 8 min after 4 runs) and catalytic universality for various substituent nitrophenols (e.g. 2-NP, 3-NP and 2,4-DNP). Although the catalytic activity was somewhat inhibited in real water samples, it still maintains a relatively high conversion efficiency of 4-NP, demonstrating the possibility for practical application.

In the reaction process, SSBC-800 interacts with BH_4^- to form surface bound hydride that subsequently attacks the adsorbed 4-NP, during which electron transfer happens from BH_4^- (electron donor) to 4-NP (electron acceptor) with SSBC-800 as the electron shuttle.

This is the first research investigating the potential of biochar as a high efficient catalyst in nitrophenol reduction, which not only broadens the application scope of biochar but also provides guidelines for further designing of carbon-based catalyst in the wastewater treatment. In addition, this smart conversion of sewage sludge into value-added material will inspire future studies to explore the biowaste as precursors for various functional materials.

Declaration of Competing Interest

We declare that we have no conflicts of interest to this work.

Acknowledgments

This study was financially supported by the National Natural Science Foundation of China (51521006, U20A20323), the Funds for Innovative Province Construction of Hunan Province of China (2019RS3012).

Supplementary materials

Supplementary material associated with this article can be found, in the online version, at doi:10.1016/j.watres.2021.117360.

References

- Cao, H., Liu, C., Cai, F., Qiao, X., Dichiaro, A.B., Tian, C., Lü, J., 2020. In situ immobilization of ultra-fine Ag NPs onto magnetic Ag@RF@Fe₃O₄ core-satellite nanocomposites for the rapid catalytic reduction of nitrophenols. *Water Res.* 179, 115882.
- Cieslik, B.M., Namieśnik, J., Konieczka, P., 2015. Review of sewage sludge management: standards, regulations and analytical methods. *J. Clean. Prod.* 90, 1–15.
- Collard, F., Blin, J., 2014. A review on pyrolysis of biomass constituents: mechanisms and composition of the products obtained from the conversion of cellulose, hemicelluloses and lignin. *Renew. Sust. Energ. Rev.* 38, 594–608.
- Das, R., Sypu, V.S., Paumo, H.K., Bhaumik, M., Maharaj, V., Maity, A., 2019. Silver decorated magnetic nanocomposite (Fe₃O₄@PPy-MAA/Ag) as highly active catalyst towards reduction of 4-nitrophenol and toxic organic dyes. *Appl. Catal. B* 244, 546–558.
- Fu, J., Wang, S., Wang, X., Yan, Y., Wang, K., Gao, M., Xu, Q., 2018. Facile preparation of highly dispersed Pt nanoparticles supported on heteroatom-containing porous carbon nanospheres and their catalytic properties for the reduction of 4-nitrophenol. *J. Porous Mat.* 25, 1081–1089.
- Fu, Y., Qin, L., Huang, D., Zeng, G., Lai, C., Li, B., He, J., Yi, H., Zhang, M., Cheng, M., Wen, X., 2019. Chitosan functionalized activated coke for Au nanoparticles anchoring: green synthesis and catalytic activities in hydrogenation of nitrophenols and azo dyes. *Appl. Catal. B* 255, 117740.
- Gao, C., An, Q., Xiao, Z., Zhai, S., Zhai, B., Shi, Z., 2018. Alginate and polyethyleneimine dually mediated synthesis of nanosilver-containing composites for efficient p-nitrophenol reduction. *Carbohydr. Polym.* 181, 744–751.
- Guo, Y., Zhang, L., Liu, X., Li, B., Tang, D., Liu, W., Qin, W., 2016. Synthesis of magnetic core-shell carbon dot@MFe₂O₄ (M = Mn, Zn and Cu) hybrid materials and their catalytic properties. *J. Mater. Chem. A* 4, 4044–4055.
- Gupta, V.K., Atar, N., Yola, M.L., Üstüindag, Z., Uzun type="Periodical", L., 2014. A novel magnetic Fe@Au core-shell nanoparticles anchored graphene oxide recyclable nanocatalyst for the reduction of nitrophenol compounds. *Water Res* 48, 210–217.
- Hu, H., Xin, J.H., Hu, H., Wang, X., 2015. Structural and mechanistic understanding of an active and durable graphene carbocatalyst for reduction of 4-nitrophenol at room temperature. *Nano Res.* 8, 3992–4006.
- Hu, X., Sun, X., Song, Q., Zhu, Y., Long, Y., Dong, Z., 2020. N,S co-doped hierarchically porous carbon materials for efficient metal-free catalysis. *Green Chem.* 22, 742–752.
- Kambo, H.S., Dutta, A., 2015. A comparative review of biochar and hydrochar in terms of production, physico-chemical properties and applications. *Renew. Sust. Energ. Rev.* 45, 359–378.
- Keown, D.M., Li, X., Hayashi, J., Li, C., 2007. Characterization of the structural features of char from the pyrolysis of cane trash using fourier transform-raman spectroscopy. *Energ. Fuel.* 21, 1816–1821.
- Kong, X., Sun, Z., Chen, M., Chen, C., Chen, Q., 2013. Metal-free catalytic reduction of 4-nitrophenol to 4-aminophenol by N-doped graphene. *Energ. Environ. Sci.* 6, 3260.
- Liu, R., Mahurin, S.M., Li, C., Unocic, R.R., Idrobo, J.C., Gao, H., Pennycook, S.J., Dai, S., 2011. Dopamine as a carbon source: the controlled synthesis of hollow carbon spheres and yolk-structured carbon nanocomposites. *Angew. Chem. Int. Ed.* 50, 6799–6802.
- McDonald-Wharry, J., Manley-Harris, M., Pickering, K., 2013. Carbonisation of biomass-derived chars and the thermal reduction of a graphene oxide sample studied using Raman spectroscopy. *Carbon* 59, 383–405.
- Narayanan, R.K., Devaki, S.J., 2015. Brawny silver-hydrogel based nanocatalyst for reduction of nitrophenols: studies on kinetics and mechanism. *Ind. Eng. Chem. Res.* 54, 1197–1203.
- Nguyen, T.B., Huang, C.P., Doong, R., 2019. Enhanced catalytic reduction of nitrophenols by sodium borohydride over highly recyclable Au@graphitic carbon nitride nanocomposites. *Appl. Catal. B* 240, 337–347.
- Oturan, M.A., Peiroten, J., Chartrin, P., Acher, A.J., 2000. Complete destruction of p-nitrophenol in aqueous medium by electro-fenton method. *Environ. Sci. Technol.* 34, 3474–3479.
- Parnaudeau, V., Dignac, M., 2007. The organic matter composition of various wastewater sludges and their neutral detergent fractions as revealed by pyrolysis-GC/MS. *J. Anal. Appl. Pyrol.* 78, 140–152.
- Periasamy, M., Thirumalaikumar, M., 2000. Methods of enhancement of reactivity and selectivity of sodium borohydride for applications in organic synthesis. *J. Organomet. Chem.* 609, 137–151.
- Qiu, Y., Ma, Z., Hu, P., 2014. Environmentally benign magnetic chitosan/Fe₃O₄ composites as reductant and stabilizer for anchoring Au NPs and their catalytic reduction of 4-nitrophenol. *J. Mater. Chem. A* 2, 13471–13478.
- Ren, X., Wang, J., Yu, J., Song, B., Feng, H., Shen, M., Zhang, H., Zou, J., Zeng, G., Tang, L., Wang, J., 2021. Waste valorization: transforming the fishbone biowaste into biochar as an efficient persulfate catalyst for degradation of organic pollutant. *J. Clean. Prod.* 291, 125225.
- Robertson, J., Ferrari, A.C., 2000. Interpretation of Raman spectra of disordered and amorphous carbon. *Phys. Rev. B* 61, 14095–14107.
- Shan, J., Sun, X., Zheng, S., Wang, T., Zhang, X., Li, G., 2019. Graphitic N-dominated nitrogen-doped carbon nanotubes as efficient metal-free catalysts for hydrogenation of nitroarenes. *Carbon* 146, 60–69.
- Smith, K.M., Fowler, G.D., Pullket, S., Graham, N.J.D., 2009. Sewage sludge-based adsorbents: a review of their production, properties and use in water treatment applications. *Water Res.* 43, 2569–2594.
- Sun, J., Fu, Y., He, G., Sun, X., Wang, X., 2014. Catalytic hydrogenation of nitrophenols and nitrotoluenes over a palladium/graphene nanocomposite. *Catal. Sci. Technol.* 4, 1742–1748.
- Syed-Hassan, S.S.A., Wang, Y., Hu, S., Su, S., Xiang, J., 2017. Thermochemical processing of sewage sludge to energy and fuel: fundamentals, challenges and considerations. *Renew. Sust. Energ. Rev.* 80, 888–913.
- Tsaneva, V.N., Kwapinski, W., Teng, X., Glowacki, B.A., 2014. Assessment of the structural evolution of carbons from microwave plasma natural gas reforming and biomass pyrolysis using Raman spectroscopy. *Carbon* 80, 617–628.
- Vaidya, M.J., Kulkarni, S.M., Chaudhari, R.V., 2003. Synthesis of p-aminophenol by catalytic hydrogenation of p-nitrophenol. *Org. Process Res. Dev.* 7, 202–208.
- Van Nguyen, C., Lee, S., Chung, Y.G., Chiang, W., Wu, K.C.W., 2019. Synergistic effect of metal-organic framework-derived boron and nitrogen heteroatom-doped three-dimensional porous carbons for precious-metal-free catalytic reduction of nitroarenes. *Appl. Catal. B* 257, 117888.
- Wang, B., Si, L., Geng, J., Su, Y., Li, Y., Yan, X., Chen, L., 2017. Controllable magnetic 3D nitrogen-doped graphene gel: synthesis, characterization, and catalytic performance. *Appl. Catal. B* 204, 316–323.
- Wang, J., Chen, H., Tang, L., Zeng, G., Liu, Y., Yan, M., Deng, Y., Feng, H., Yu, J., Wang, L., 2018. Antibiotic removal from water: a highly efficient silver phosphate-based Z-scheme photocatalytic system under natural solar light. *Sci. Total Environ.* 639, 1462–1470.
- Wang, H., Guo, W., Liu, B., Wu, Q., Luo, H., Zhao, Q., Si, Q., Sseguya, F., Ren, N., 2019. Edge-nitrogenated biochar for efficient peroxydisulfate activation: an electron transfer mechanism. *Water Res* 160, 405–414.
- Xi, J., Xiao, J., Xiao, F., Jin, Y., Dong, Y., Jing, F., Wang, S., 2016. Mussel-inspired functionalization of cotton for nano-catalyst support and its application in a fixed-bed system with high performance. *Sci. Rep.* 6, 21904.
- Xia, J., He, G., Zhang, L., Sun, X., Wang, X., 2016. Hydrogenation of nitrophenols catalyzed by carbon black-supported nickel nanoparticles under mild conditions. *Appl. Catal. B* 180, 408–415.
- Xu, Z., Deng, X., Zhang, S., Shen, Y., Shan, Y., Zhang, Z., Luque, R., Duan, P., Hu, X., 2020. Benign-by-design N-doped carbonaceous materials obtained from the hydrothermal carbonization of sewage sludge for supercapacitor applications. *Green Chem.* 22, 3885–3895.
- Yang, F., Chi, C., Wang, C., Wang, Y., Li, Y., 2016. High graphite N content in nitrogen-doped graphene as an efficient metal-free catalyst for reduction of nitroarenes in water. *Green Chem* 18, 4254–4262.
- Yang, Y., Li, X., Zhou, C., Xiong, W., Zeng, G., Huang, D., Zhang, C., Wang, W., Song, B., Tang, X., Li, X., Guo, H., 2020. Recent advances in application of graphitic carbon nitride-based catalysts for degrading organic contaminants in water through advanced oxidation processes beyond photocatalysis: a critical review. *Water Res.* 184, 116200.
- Yang, Y., Zhang, W., Ma, X., Zhao, H., Zhang, X., 2015b. Facile construction of mesoporous N-doped carbons as highly efficient 4-nitrophenol reduction catalysts. *ChemCatChem* 7, 3454–3459.
- Yang, G., Zhang, G., Wang, H., 2015a. Current state of sludge production, management, treatment and disposal in China. *Water Res* 78, 60–73.
- Yu, J., Tang, L., Pang, Y., Zeng, G., Wang, J., Deng, Y., Liu, Y., Feng, H., Chen, S., Ren, X., 2019. Magnetic nitrogen-doped sludge-derived biochar catalysts for persulfate activation: internal electron transfer mechanism. *Chem. Eng. J.* 364, 146–159.
- Zhang, J., Lü, F., Zhang, H., Shao, L., Chen, D., He, P., 2015. Multiscale visualization of the structural and characteristic changes of sewage sludge biochar oriented towards potential agronomic and environmental implication. *Sci. Rep.* 5, 9406.
- Zhang, P., Zheng, S., Liu, J., Wang, B., Liu, F., Feng, Y., 2018. Surface properties of activated sludge-derived biochar determine the facilitating effects on *Geobacter* cultures. *Water Res* 142, 441–451.
- Zhang, Z., Sun, T., Chen, C., Xiao, F., Gong, Z., Wang, S., 2014. Bifunctional nanocatalyst based on three-dimensional carbon nanotube-graphene hydrogel supported Pd Nanoparticles: one-pot synthesis and its catalytic properties. *ACS Appl. Mater. Inter.* 6, 21035–21040.